Planar Terahertz Photonics Mediated by Liquid Crystal Polymers

Zhi-Xiong Shen, Ming-Jie Tang, Peng Chen, Sheng-Hang Zhou, Shi-Jun Ge, Wei Duan, Ting Wei, Xiao Liang, Wei Hu,* and Yan-Qing Lu*

Terahertz (THz) band is expected to satisfy the ever-increasing demand for high-capacity wireless data transfer. Multifunctional photonic devices with compactness and low loss are highly pursued for future THz communications. Here, a strategy for planar THz photonics is proposed that enables free wavefront manipulation with submillimeter thin liquid crystal polymer (LCP) films. Such elements work on the spatial geometric phase modulation, which is accomplished by preprogramming the axis orientations of LCP. The LCP monomers follow the guidance of local photoalignment agent and are further polymerized under UV exposure at the existence of a doped photo-initializer. Thanks to the high resolution and excellent flexibility of the photopatterning technique, THz elements with versatile functions can be realized. As examples, waveplates, polarization gratings, and lenses, which are suitable for the polarization control, beam deflecting, focusing, or collimating, are demonstrated. Due to the intrinsic flexibility of LCP films, an *f*-tunable lens enabled by mechanically induced deformation is exhibited. Specific mode generators for vortices and Bessel beams are also presented, which can function as separate channels for the mode division multiplexing in THz communications. This work provides a robust platform for fabricating integrated, low-loss, and tunable THz elements suitable for the advanced THz apparatuses.

1. Introduction

The past decades have witnessed the explosively increasing data traffic on wireless channels, which is expected to reach

Dr. Z.-X. Shen, M.-J. Tang, Dr. P. Chen, S.-H. Zhou, Dr. S.-J. Ge,
Dr. W. Duan, T. Wei, Prof. W. Hu, Prof. Y.-Q. Lu
National Laboratory of Solid State Microstructures
Key Laboratory of Intelligent Optical Sensing and Manipulation
College of Engineering and Applied Sciences
and Collaborative Innovation Center of Advanced Microstructures
Nanjing University
Nanjing 210093, China
E-mail: huwei@nju.edu.cn; yqlu@nju.edu.cn
Dr. Z.-X. Shen, Dr. P. Chen, Dr. S.-J. Ge, Prof. W. Hu
Institute for Smart Liquid Crystals
JITRI
Changshu 215500, China
Prof. X. Liang
Department of Chemistry
Tsinghua University
Beijing 100084, China

The ORCID identification number(s) for the author(s) of this article can be found under https://doi.org/10.1002/adom.201902124.

77 exabytes per month by 2022.[1] To adapt this trend, a large channel capacity over 100 Gbit s^{-1} is indispensable for the future wireless networks. Terahertz (THz) wave possesses a carrier frequency (0.1–10 THz) much higher than currently adopted RF band, thus is envisioned as the most likely candidate for future high-capacity wireless communications.[2–6] However, THz wave is the most elusive band in electromagnetic spectra. Many THz technologies are still far from maturation compared with their electrical or optical counterparts. Especially, the THz band exceeds the cut-off frequency of semiconductors involved in electronic amplifiers and mixers. Therefore, present electronic elements in RF systems are no longer compatible in this new band.[7] Facing this challenge, scientists start to exploit photonic solutions. In initial researches, refractive and reflective elements of specific geometries are introduced to generate spatial optical path differences for wavefront control.[8] Unfortunately, the bulky and heavy architectures distinctly restrict the minimization and integration of THz photonics. Recently, THz planar photonics are presented based on the wavefront manipulation arising from particularly designed subwavelength resonator units, i.e., metasurfaces.[9,10] By this means, the amplitude, phase, and polarization of THz wave can be freely tailored.[11–22] However, the high Ohmic loss of plasmonic metasurface results in a significantly suppressed efficiency. The newly developed dielectric[23–25] and multilayered plasmonic metasurfaces[26–28] can drastically improve the efficiency, but result in the complexity of design and fabrication, hindering their practical applications. To meet the requirements of future THz communications, exploring planar THz photonics with simple configuration, low loss, and low cost is imperative.

Liquid crystal (LC) features a broadband birefringence from visible to microwave and pronounced responsivity to external fields including thermal, optical, electromagnetical, etc. Beyond information displays, LC has also been employed in broad photonic applications, e.g., optical phased arrays, telecom components, and optical mode converters.[29–36] Along with the emergence of large-birefringence LCs and high-transparency electrodes in THz regime,[37–40] tunable filters,[41,42] phase shifters,[43,44] and waveplates[45] were developed subsequently.

**ADVANCED
SCIENCE NEWS**
www.advancedsciencenews.com

**ADVANCED
OPTICAL
MATERIALS**
www.advopticalmat.de

Via further introducing the photopatterning technique, multifunctional geometric phase elements, such as vortex beam generators and spin-selected lenses, were accomplished.[46,47] Due to their electro-optical tunability, the efficiency can be optimized for certain working frequencies. However, the large thickness of LC layer, typically hundreds of microns, for accumulating sufficient phase retardation causes the drawbacks of slow response (in seconds scale) and high operating voltage. Actually, for many conditions, only a narrow band or even a single frequency is involved. In these cases, electric tuning is not necessary. Similar to LCs, liquid crystal polymers (LCPs) possess broadband dielectric anisotropy.[48,49] Thanks to the polymerization, their stability is greatly improved. The superior low dielectric loss of LCP makes it an alternative of the polyimide as the flexible substrate for communications operated at higher carrier frequencies.[50] It suggests that the LCP can serve as both specific phase modulator and substrate after patterned. This integration may supply a compact solution for THz photonics with significantly reduced insertion loss. Corresponding research has rarely been explored in THz regime yet. It will be a steady step toward THz photonics.

In this paper, we propose a compact and flexible platform for planar THz photonics based on photopatterned LCP films. The geometric phase of LCP elements can be manipulated point to point via spatially controlling LC directors. Therefore, versatile functions can be freely designed. After infiltrated into a photopatterned cell, the LCP precursor follows the guidance of local alignment. Followed by UV polymerization and separation from the silica substrates, a free-standing and flexible LCP film with a submillimeter thickness is obtained. The LCP faithfully retains the original orientations. These films can work as multifunctional THz elements. Herein, waveplates, deflectors, lenses, and specific mode converters are demonstrated and their properties are systematically investigated with a THz time-domain spectroscopy (THz-TDS) and a scanning near-field THz microscope (SNTM) system. They may play important roles in THz communications for polarization control, beam scanning, beam forming, and coupling. Besides, the flexibility of LCP films enables the elements a deformation-induced tunability. This is a solid move toward various apparatuses for future THz applications.

2. Results and Discussion

Geometric phase, namely Pancharatnam–Berry phase,[51] is originated from the photonic spin-orbit interaction[52] and generated from the geometry of the anisotropic media[53,54] (e.g., optical axes of crystals/LCs or orientations of metasurface resonators). When circular polarization (CP) incidents, the output wave can be expressed as

$$\mathbf{E}_{out} = \mathbf{J} \cdot \chi^{(\pm)} = \cos\zeta \cdot \chi^{(\pm)} - i\sin\zeta \cdot \exp(\pm i2\alpha) \cdot \chi^{(\mp)} \tag{1}$$
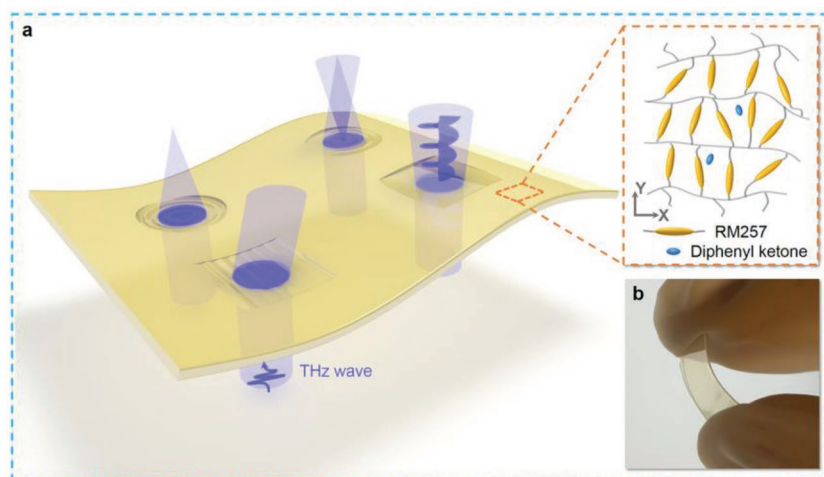

Figure 1. Planar THz photonics enabled by photopatterned LCPs. a) Schematic illustration of the beam deflector, lens, Bessel and vortex beam generator assembled on a single flexible LCP film. Inset shows the polymer chain configuration. b) Photograph of the sample.

where **J** represents the Jones matrix of the anisotropic medium with a rotation angle α, ζ is half of the phase difference between two orthogonal linearly polarized components, $\chi^{(+)}$ and $\chi^{(-)}$ represent left circular polarization (LCP) and right circular polarization (RCP), respectively. A full phase control of 0–2π can be continuously realized by changing α from 0 to π with a CP conversion. According to Equation (1), the polarization conversion efficiency (PCE) is maximized at the half-wave condition. In this case, a uniform geometric phase is encoded to the incident CP, meanwhile the CP is totally reversed. If α is arbitrarily manipulated, one can freely control the phase profile of the output. Thus, planar photonics with versatile functions could be achieved.

The dominant component of LCP is a polymerizable LC monomer. Via a photopatterning technique (see Section S1, Supporting Information), its in-plane orientation can be arbitrarily and precisely controlled. It makes LCP an excellent candidate for geometric phase modulation. **Figure 1**a schematically illustrates four different elements (beam deflector, lens, Bessel, and vortex beam generator) with their functions presented as well. The polymer chain configuration is shown in the inset. Despite that the monomers are crosslinked, they remain the original orientations. In our work, the LCP precursor is composed of 99.7 wt% nematic LC monomer RM257 and 0.3 wt% photo-initializer Diphenyl ketone. After UV polymerization, the precursor turns to a densely crosslinked network.[55] The photograph of a 350 μm thick film (Figure 1b) vividly exhibits its flexibility.

For such LCP elements, the phase modulation directly stems from the orientation of optical axes. Its efficiency is determined by the phase retardation $\varphi_p = 2\pi\Delta nd/\lambda$, where Δn is the birefringence, d is the film thickness, and λ is the incident wavelength. THz refractive indices (n_o and n_e) and absorption coefficients (κ_o and κ_e) of the LCP are measured using a THz-TDS with a transmission polarization analysis module (**Figure 2**a). The average birefringence is 0.17 from 0.4 to 3.0 THz and the absorption loss is moderate (Figure S2, Supporting Information). On the basis of above data, the dependency of φ_p on
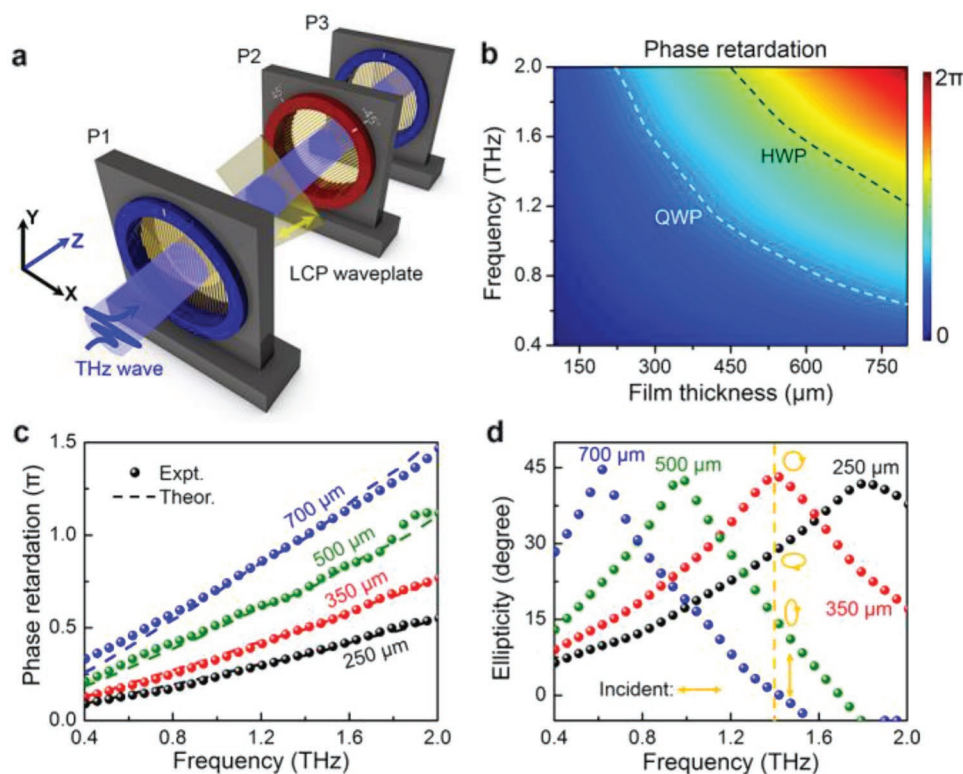
Figure 2. THz polarization characterizations of LCP waveplates. a) Experimental setup of a THz-TDS with a transmission polarization analysis module. P represents metal grating polarizers. The grating vectors of P1 and P3 are both orientated along *x*-axis to select *x*-polarization. Whereas the grating vector of P2 is altered between 45° or −45° to select E_e and E_o, respectively. The LCP orientation is 45° as indicated by the yellow arrow. b) Theoretical dependency of phase retardation on frequency and film thickness. c and d) Frequency-dependent phase retardation (c) and ellipticity (d) at four different film thicknesses. The orange arrows in (d) depict the polarization evolution at 1.4 THz.

frequency and *d* is calculated and exhibited in Figure 2b. As expected, φ_p increases along with frequency and *d*, respectively. The white and black dashed lines label the quarter-wave (i.e., $\varphi_p = 0.5\pi$) and half-wave (i.e., $\varphi_p = \pi$) conditions, separately. For demonstration, several homogeneously aligned LCP films are fabricated and tested. φ_p and ellipticity (Section S2, Supporting Information) of 250, 350, 500, and 700 µm thick samples are revealed in Figure 2c,d, respectively. It should be noticed that the maximum thickness for a single cell is restricted to 350 µm, thereby the latter two are double layered. The measured data match well with the calculations in Figure 2c, indicating a qualified alignment. Corresponding polarization evolution at 1.4 THz is presented in Figure 2d. The proposed strategy provides a practical solution for polarization manipulation, which is a key requirement in THz communication, sensing, and imaging.

Deflector and lens are important elements for beam forming, steering, focusing, and collimating in the THz communications. Polarization gratings can deflect beams to certain angles. Its phase profile is expressed by

$$\varphi_D = -2\pi x \sin\theta_d / \lambda \qquad (2)$$

where θ_d is the deflection angle. Here, we encode the phase into LCP orientations and a deflector with $\theta_d = 12°$ at 1.0 THz is fabricated. An SNTM system (**Figure 3**a) is used to characterize

the deflector. Figure 3b presents the photo of the deflector and corresponding theoretical phase profile. It is obvious that the LC directors vary continuously, resulting in periodic phase changes. Figure 3c shows the THz fields in the *xz*- and *xy*-planes for incident RCP and LCP waves, separately. According to the transverse intensity distribution (Figure 3d), the θ_d are −11.3°/12.2° for RCP/LCP waves, respectively. The little deviation is mainly due to a slightly tilt incidence of the THz beam. Waves of opposite spin states are deflected in mirrored trajectories, as they experience conjugated blazed phases. Via varying the period of polarization gratings, the deflection angle can be freely tuned.

The phase profile of a spherical lens is given by

$$\varphi_L = -2\pi \left(\sqrt{f^2 + r^2} - f \right) / \lambda \qquad (3)$$

where *r* is the polar radius and *f* represents the focal length. We fabricate a lens with *f* = 15 mm at 1.0 THz. For simple demonstration, both the deflector and lens are made by 350 µm thick LCP films. The photo and phase diagram in Figure 3e reveal the gradually and axially changes of both directors and phase of the lens. The THz fields at four frequencies from 0.6 to 1.2 THz with a step of 0.2 THz are simulated and measured (Figures S3 and S4, Supporting Information). Figure 3f demonstrates the THz fields (at 0.6 and 1.2 THz) in the *xz*-plane and respective focal planes. As shown in Figure 3g, *f* increases with frequency,

1902124 (3 of 8)

**ADVANCED
SCIENCE NEWS**

www.advancedsciencenews.com

**ADVANCED
OPTICAL
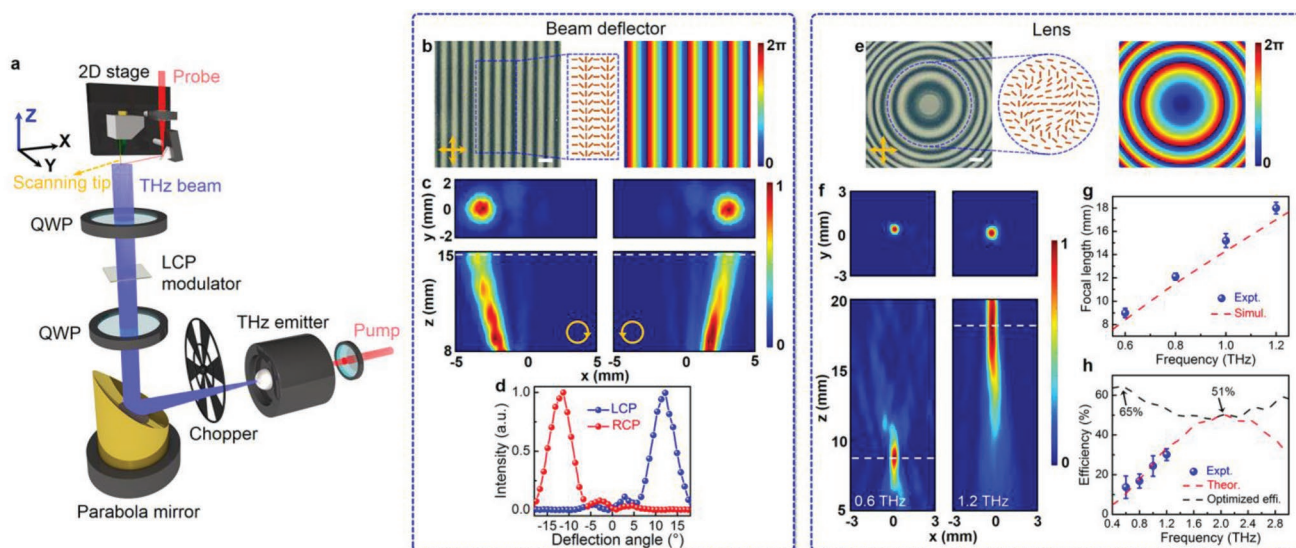MATERIALS**

www.advopticalmat.de

Figure 3. THz elements for beam deflecting and focusing. a) Experimental setup of the SNTM system. b) Photo of the deflector under crossed polarizers (indicated by two yellow arrows) with local LC orientations indicated by orange bars and corresponding phase diagram. Scale bar: 1 mm, same hereinafter. c) Normalized THz fields in the xy- (z = 15 mm) and xz-plane at 1.0 THz. d) Transverse intensity distributions along the dashed lines in (c). e) Photo of the lens and corresponding phase diagram. f) Measured THz fields in the xz-plane and corresponding focal planes at 0.6 and 1.2 THz. g and h) Dependencies of focal length (g) and efficiency (h) on frequency.

which is consistent with the simulation result. The insertion loss of produced lens comes from two attributions: the mismatch of half-wave condition and the intrinsic absorption. For a target frequency, the efficiency, which equals to the product of PCE and THz transmission, can be optimized via adjusting d (see Section S3, Supporting Information). Figure 3h shows the calculated efficiency when d is 350 μm (red dashed line). From the calculation, the maximum efficiency reaches 51% at 2.1 THz. Due to the testing band limitation of the SNTM system (0.5–1.4 THz), only four frequencies (blue dots) in this range are measured. The efficiency varies from 13.7% to 30.1% and matches well with the calculation. For the lower frequency band, a stacking film strategy should be adopted to approach the half-wave condition. However, the increased thickness brings extra absorption loss. Fortunately, the absorption decreases exponentially with the reduced frequency, making the optimized efficiency keeps over 50% in the whole range with a maximum of 65% at 0.5 THz (black dashed line). This efficiency can be further enhanced via exploring other LCP materials with larger birefringence and lower absorption. For a comparison, the single-layer plasmonic metasurfaces possess a theoretically limited resonant efficiency of 25%.[56,57] The unavoidable substrates of THz elements bring extra loss (e.g., the 1 mm thick silica transmits only 64% at 1.0 THz), resulting in a severely suppressed efficiency. Here, the free-standing LCP film significantly improves the efficiency of THz photonics.

The flexibility of the film brings LCP elements the merit of deformation induced tunability. As a proof of concept, a 250 μm thick LCP cylindrical lens is demonstrated. Its phase profile is shown as

$$\varphi_C = -2\pi\left(\sqrt{f^2 + x^2} - f\right)/\lambda \tag{4}$$

When such a lens is compressed, it will turn from flat (**Figure 4**a) to bending (Figure 4b) state. Along with the bending

strain (ε) increasing, the 0–2π phase alternation changes more rapidly, resulting in an increased refraction angle. And f is shortened accordingly (detailed in Section S4, Supporting Information). Numerical simulations (Figure 4d) and experimental characterizations (Figure 4e) at 1.0 THz under four different ε are carried out. f continuously decreases with ε increasing. The difference between measurements and simulations (Figure 4f) is attributed to the deviation from an ideal sinusoidal model. The deformation induced tunability is meaningful to various THz modulations, especially for active beam steering, focusing, and collimating.

Besides the higher carrier frequency, the capacity of communications could also be enhanced by introducing individual channels to realize a mode division multiplexing (MDM).[58,59] These modes are featured by specific spatial intensity or phase distributions, which could transmit separately without crosstalk. Among them, Bessel and vortex modes (Sections S5 and S6, Supporting Information) carrying quantized orbit angular momentum (OAM) have attracted intensive attentions. Herein, a zeroth Bessel beam generator is fabricated and tested (**Figure 5**a). Its phase is wroten as

$$\varphi_A = -2\pi r \sin\theta_t / \lambda \tag{5}$$

where θ_t is the deflection angle in the radius direction (designed $\theta_t = 9.5°$ at 1 THz). The diffraction-free property with a focal depth over 10 mm is verified. The THz field in the xy-plane clearly shows a Bessel-type distribution with a central spot surrounded by concentric rings. Higher order Bessel beams carrying OAM modes can function as independent channels. For simple domenstration, we use LCP q-plates[60] to generate different OAM modes, which could encode the target spiral phase to the transmitted plane wave. q-Plates with topological charges m = 1, 2, and 4 are fabricated and
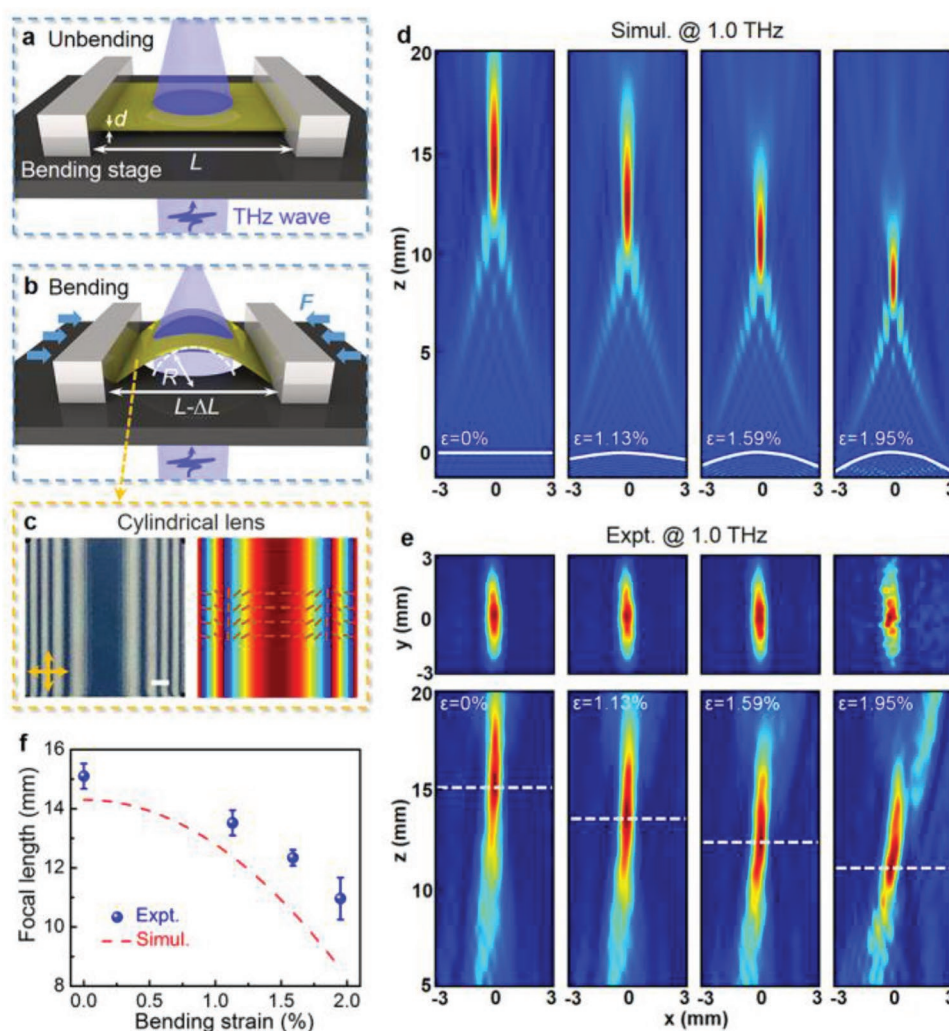
Figure 4. Mechanical deformation induced *f*-tunable lens. a and b) Schematic illustrations of the lens at flat (a) and bending (b) state. *L* denotes the original film length, ΔL is the length reduction at the bending state, and *R* is the radius of curvature. c) Photo of the cylindrical lens and corresponding phase diagram with local LC orientations. d) Simulated THz fields in the *xz*-plane with a bending strain of 0%, 1.13%, 1.59%, and 1.95%, respectively. The white lines depict the bending shape. e) Measured THz fields in the *xz*-plane and corresponding focal planes at 1.0 THz. f) Dependency of focal length on bending strain.

characterized (Figure 5b–d). *m* can be directly read from the number of azimuthal $0–2\pi$ alternations. In our experiments, the designed spiral phases are faithfully loaded by the THz wave. Theoretically, OAM modes possess infinite *m*, exhibiting great potentials in enhancing the bandwidth of wireless communications.

The geometric phase, which determines the function of generated LCP elements, exhibits a double relationship with local LC directors. Thus, it can be directly encoded without additional simulations for structural parameter optimizations. The target orientations are fabricated via a simple process of polarized photo exposure. Monomers will self-assemble to follow the guidance of local alignment. Photopatterning possesses the merits of high resolution and arbitrary image output, enabling the designed phase distribution to be faithfully recorded into LCP elements. LCPs are commercially available and cost-efficient materials with

mature coating and patterning techniques. It supplies a practical and affordable strategy for the large-scale fabrication of THz photonics. The efficiency at objective frequency can be optimized via varying the film thickness. The proposed LCP elements exhibit a device efficiency over 50% in a broad THz band, which is the highest one at present and could be further improved by exploiting higher-transparency LCPs in future. Via introducing specific chiral structures,[54,61] the elements can achieve a same high efficiency over a broadband. It should be noticed that the photopatterned LCPs can serve as substrates for other THz elements, further reducing the loss of various THz apparatuses. The submillimeter thickness of LCP elements endows them a pronounced flexibility. Through mechanically induced deformation, tunability is brought to these devices with static microstructures, which is of great significance for dynamic beam steering and focusing.[62,63]
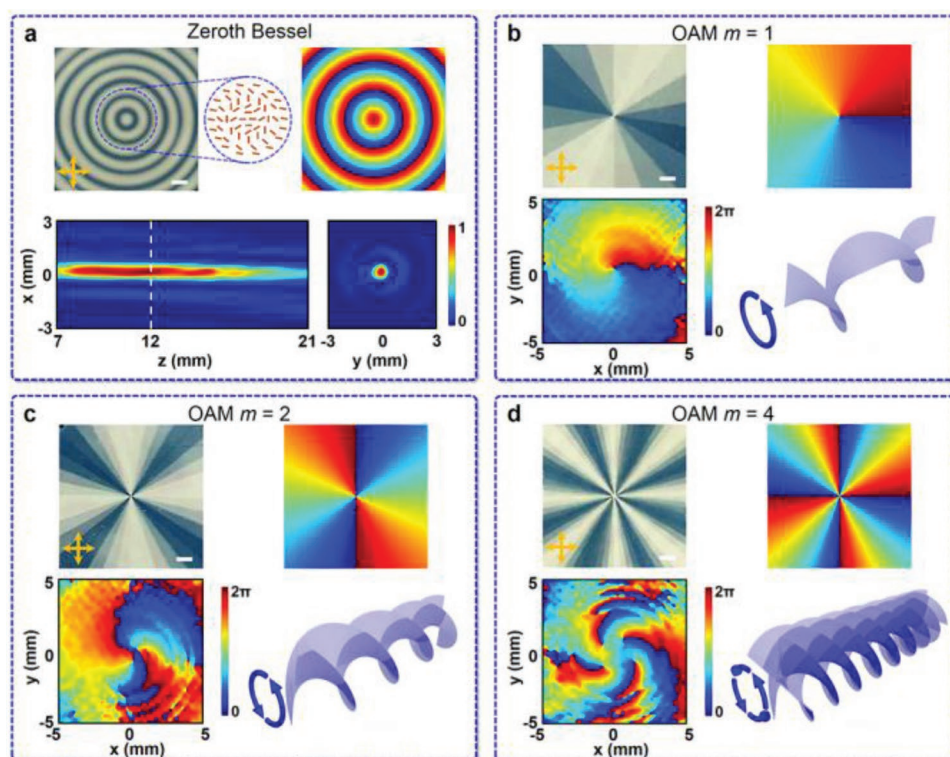
**ADVANCED
SCIENCE NEWS**
www.advancedsciencenews.com

**ADVANCED
OPTICAL
MATERIALS**
www.advopticalmat.de

Figure 5. THz Bessel and vortex mode generators. a) Photo, phase diagram, and measured THz fields in the *xz*- and *xy*-plane (*z* = 12 mm at 1.0 THz) of the zeroth Bessel mode generator. b–d) Photos, phase diagrams of vortex mode generators with *m* = 1 (b), *m* = 2 (c), and *m* = 4 (d), respectively; and measured phase distributions and 3D schemes of produced vortices.

3. Conclusion

In summary, planar THz elements such as waveplates, deflectors, lenses, and specific mode converters are demonstrated via encoding geometric phase into LCP films. Fundamental functions in THz wireless communications including polarization control, beam scanning, beam forming, and coupling are realized. The freely programmable LCP orientations enable the on-demand THz beam tailoring, facilitating the design, and fabrication of versatile THz elements. The proposed LCP strategy provides a novel platform for THz photonics with merits of easy fabrication, low cost and loss, compactness, and tunability. This work broadens the applications of LCPs and may inspire various advanced apparatuses for THz communication, imaging, and sensing.

4. Experimental Section

Sample Fabrication: The fabrication procedure of the LCP functional film is schematically shown in Figure S9, Supporting Information. LC monomer RM257 (Nanjing Murun Advanced Material Co. Ltd., China; chemical structure shown in Figure S10, Supporting Information, T_g = 73 °C, T_c = 131 °C) was mixed with the photo-initiator Diphenyl ketone (Shanghai Lingfeng Chemical Reagent Co. Ltd., China; chemical structure shown in Figure S11, Supporting Information) at a ratio of 99.7 wt% to 0.3 wt%. The LCP precursor was stirred at 120 °C for 60 min. Fused silica substrates were ultrasonically bathed and O-plasma treated for 10 min. They were spin-coated at 3000 rpm for 30 s with

SD1 solution (Dai-Nippon Ink and Chemicals, Japan; chemical structure shown in Figure S12, Supporting Information) and baked at 100 °C for 10 min to remove the solvent. Then the two substrates were assembled with Mylar spacer to form a cell. After a photopatterning process, the precursor was infiltrated at 140 °C and slowly cooled down to 75 °C. After polymerization under a UV lamp for 30 min, the film was taken out from the cell.

Numerical Simulation: Simulations of LCP elements were carried out using a commercial software, Lumerical FDTD Solutions. Due to the geometric symmetry of the lens, the model in the *xz*-plane was established to simplify the simulation. It was divided into small polygons, in which the eight vertex coordinates were determined by the sinusoidal bending shape. The LC was set as a diagonal dielectric material with n_o = 1.62 (diagonal elements *xx* and *yy*) and n_e = 1.79 (diagonal element *zz*). The LC director distributions were set by an LC orientation module, where the azimuth and tilt angle jointly determined the specific LC orientation. A plane wave (0.6–1.2 THz) was incident along *z*-axis.

Characterizations: A THz-TDS (Advantest Corporation, Japan; TAS7400SP) and an SNTM system (Terahertz Photonics Co. Ltd., China; TP800) were utilized for THz performance characterizations (Section S7, Supporting Information). The SNTM setup was based on the photoconductive antenna THz generation and detection. A pair of metallic electrodes were deposited on a semiconductor substrate to function as the THz source. When a femtosecond laser pulse pumped it, the inner electrons oscillated and radiated THz. The principle for detection was the inverse of emission. When the THz wave illuminated, the photo-generated carriers excited by the probe laser beam moved directionally and a varying current was generated. Through detecting the current, the time-domain THz signal can be restored. THz intensity and phase can be derived using the fast Fourier transformation. The scanning tip was fixed in a motorized stage (Figure 3a), which can move

**ADVANCED
SCIENCE NEWS**

www.advancedsciencenews.com

**ADVANCED
OPTICAL
MATERIALS**

www.advopticalmat.de

in the xy-plane to record the E_x field with a step size of 0.25 mm. The sample moved along z-axis with a step size of 1 mm to capture the E_x field in the xz-plane. Then an interpolation algorithm was adopted to obtain the measured THz fields.

[1] Cisco VNI Mobile Forecast. https://www.cisco.com/c/en/us/solutions/collateral/service-provider/visual-networking-index-vni/white-paper-c11-738429.html.

[2] X. C. Zhang, J. Xu, Introduction to THz Wave Photonics, Springer, Cham, Switzerland 2010.

[3] T. Kleine-Ostmann, T. Nagatsuma, J. Infrared, Millim., Terahertz Waves 2011, 32, 143.

[4] H. J. Song, T. Nagatsuma, IEEE Trans. Terahertz Sci. Technol. 2011, 1, 256.

[5] S. Koenig, D. Lopez-Diaz, J. Antes, F. Boes, R. Henneberger, A. Leuther, A. Tessmann, R. Schmogrow, D. Hillerkuss, R. Palmer, T. Zwick, C. Koos, W. Freude, O. Ambacher, J. Leuthold, I. Kallfass, Nat. Photonics 2013, 7, 977.

[6] I. F. Akyildiz, J. M. Jornet, C. Han, Phys. Commun. 2014, 12, 16.

[7] T. Nagatsuma, G. Ducournau, C. C. Renaud, Nat. Photonics 2016, 10, 371.

[8] J. B. Masson, G. Gallot, Opt. Lett. 2006, 31, 265.

[9] N. Yu, P. Genevet, M. A. Kats, F. Aieta, J. P. Tetienne, F. Capasso, Z. Gaburro, Science 2011, 334, 333.

[10] N. Yu, F. Capasso, Nat. Mater. 2014, 13, 139.

[11] H. T. Chen, W. J. Padilla, J. M. O. Zide, A. C. Gossard, A. J. Taylor, R. D. Averitt, Nature 2006, 444, 597.

[12] D. Hu, X. Wang, S. Feng, J. Ye, W. Sun, Q. Kan, P. J. Klar, Y. Zhang, Adv. Opt. Mater. 2013, 1, 186.

[13] N. K. Grady, J. E. Heyes, D. R. Chowdhury, Y. Zeng, M. T. Reiten, A. K. Azad, A. J. Taylor, D. A. Dalvit, H. T. Chen, Science 2013, 340, 1304.

[14] L. Cong, N. Xu, J. Gu, R. Singh, J. Han, W. Zhang, Laser Photonics Rev. 2014, 8, 626.

[15] R. H. Fan, Y. Zhou, X. P. Ren, R. W. Peng, S. C. Jiang, D. H. Xu, X. Xiong, X. R. Huang, M. Wang, Adv. Mater. 2015, 27, 1201.

[16] L. H. Gao, Q. Cheng, J. Yang, S. J. Ma, J. Zhao, S. Liu, H. B. Chen, Q. He, W. X. Jiang, H. F. Ma, Q. Y. Wen, L. J. Liang, B. B. Jin, W. W. Liu, L. Zhou, J. Q. Yao, P. H. Wu, T. J. Cui, Light: Sci. Appl. 2015, 4, e324.

[17] M. Manjappa, Y. K. Srivastava, L. Cong, I. Al-Naib, R. Singh, Adv. Mater. 2017, 29, 1603355.

[18] L. Cong, Y. K. Srivastava, H. Zhang, X. Zhang, J. Han, R. Singh, Light: Sci. Appl. 2018, 7, 28.

[19] Q. Wang, E. Plum, Q. Yang, X. Zhang, Q. Xu, Y. Xu, J. Han, W. Zhang, Light: Sci. Appl. 2018, 7, 25.

[20] L. Cong, N. Xu, J. Han, W. Zhang, R. Singh, Adv. Mater. 2015, 27, 6630.

[21] L. Cong, N. Xu, W. Zhang, R. Singh, Adv. Opt. Mater. 2015, 3, 1176.

[22] L. Cong, P. Pitchappa, C. Lee, R. Singh, Adv. Mater. 2017, 29, 1700733.

[23] S. Jahani, Z. Jacob, Nat. Nanotechnol. 2016, 11, 23.

[24] D. Headland, E. Carrasco, S. Nirantar, W. Withayachumnankul, P. Gutruf, J. Schwarz, D. Abbott, M. Bhaskaran, S. Sriram, J. Perruisseau-Carrier, ACS Photonics. 2016, 3, 1019.

[25] H. Zhang, X. Zhang, Q. Xu, C. Tian, Q. Wang, Y. Xu, Y. Li, J. Gu, Z. Tian, C. Ouyang, X. Zhang, C. Hu, J. Han, W. Zhang, Adv. Opt. Mater. 2018, 6, 1700773.

[26] S. Liu, Q. Cheng, Q. Xu, T. Q. Wang, L. L. Du, K. Luan, Y. H. Xu, D. Bao, X. J. Fu, J. G. Han, Adv. Opt. Mater. 2016, 4, 384.

[27] S. Liu, A. Noor, L. L. Du, L. Zhang, Q. Xu, K. Luan, T. Q. Wang, Z. Tian, W. X. Tang, J. G. Han, ACS Photonics. 2016, 3, 1968.

[28] M. Jia, Z. Wang, H. Li, X. Wang, W. Luo, S. Sun, Y. Zhang, Q. He, L. Zhou, Light: Sci. Appl. 2019, 8, 16.

[29] D. Resler, D. Hobbs, R. Sharp, L. Friedman, T. Dorschner, Opt. Lett. 1996, 21, 689.

[30] Z. Zhang, Z. You, D. Chu, Light: Sci. Appl. 2014, 3, e213.

[31] P. Chen, S. J. Ge, W. Duan, B. Y. Wei, G. X. Cui, W. Hu, Y. Q. Lu, ACS Photonics. 2017, 4, 1333.

[32] P. Chen, L. L. Ma, W. Hu, Z. X. Shen, H. K. Bisoyi, S. B. Wu, S. J. Ge, Q. Li, Y. Q. Lu, Nat. Commun. 2019, 10.

[33] J. Kim, C. Oh, S. Serati, M. J. Escuti, Appl. Opt. 2011, 50, 2636.

[34] K. Gao, H. H. Cheng, A. K. Bhowmik, P. J. Bos, Opt. Express 2015, 23, 26086.

[35] Z. He, F. Gou, R. Chen, K. Yin, T. Zhan, S. T. Wu, Crystals 2019, 9, 292.

[36] K. Yin, Y. H. Lee, Z. He, S. T. Wu, Opt. Express 2019, 27, 5814.

[37] L. Wang, X. W. Lin, X. Liang, J. B. Wu, W. Hu, Z. G. Zheng, B. B. Jin, Y. Q. Qin, Y. Q. Lu, Opt. Mater. Express 2012, 2, 1314.

[38] Y. Wu, X. Ruan, C. H. Chen, Y. J. Shin, Y. Lee, J. Niu, J. Liu, Y. Chen, K. L. Yang, X. Zhang, J. H. Ahn, H. Yang, Opt. Express 2013, 21, 21395.

[39] C. S. Yang, T. T. Tang, P. H. Chen, R. P. Pan, P. Yu, C. L. Pan, Opt. Lett. 2014, 39, 2511.

[40] Y. Du, H. Tian, X. Cui, H. Wang, Z. X. Zhou, J. Mater. Chem. C 2016, 4, 4138.

[41] Z. X. Shen, S. H. Zhou, S. J. Ge, W. Duan, P. Chen, L. Wang, W. Hu, Y. Q. Lu, Opt. Lett. 2018, 43, 4695.

[42] Z. X. Shen, S. H. Zhou, S. J. Ge, W. Hu, Y. Q. Lu, Appl. Phys. Lett. 2019, 114, 041106.

[43] C. F. Hsieh, R. P. Pan, T. T. Tang, H. L. Chen, C. L. Pan, Opt. Lett. 2006, 31, 1112.

[44] Y. Ji, F. Fan, S. Xu, J. Yu, S. Chang, Nanoscale 2019, 11, 4933.

**ADVANCED
SCIENCE NEWS**

www.advancedsciencenews.com

**ADVANCED
OPTICAL
MATERIALS**

www.advopticalmat.de

[45] L. Wang, X. W. Lin, W. Hu, G. H. Shao, P. Chen, L. J. Liang, B. B. Jin, P. H. Wu, H. Qian, Y. N. Lu, X. Liang, Z. G. Zheng, Y. Q. Lu, *Light: Sci. Appl.* **2015**, *4*, e253.

[46] S. J. Ge, P. Chen, Z. X. Shen, W. F. Sun, X. K. Wang, W. Hu, Y. Zhang, Y. Q. Lu, *Opt. Express* **2017**, *25*, 12349.

[47] Z. Shen, S. Zhou, S. Ge, W. Duan, L. Ma, Y. Lu, W. Hu, *Opt. Express* **2019**, *27*, 8800.

[48] J. Kim, Y. Li, M. N. Miskiewicz, C. Oh, M. W. Kudenov, M. J. Escuti, *Optica* **2015**, *2*, 958.

[49] M. J. Tang, P. Chen, W. L. Zhang, A. M. Tam, V. G. Chigrinov, W. Hu, Y. Q. Lu, *Opt. Express* **2016**, *24*, 25510.

[50] G. T. Hwang, D. Im, S. E. Lee, J. Lee, M. Koo, S. Y. Park, S. Kim, K. Yang, S. J. Kim, K. Lee, K. J. Lee, *ACS Nano* **2013**, *7*, 4545.

[51] M. V. Berry, *J. Mod. Opt.* **1987**, *34*, 1401.

[52] K. Y. Bliokh, F. J. Rodríguez-Fortuño, F. Nori, A. V. Zayats, *Nat. Photonics* **2015**, *9*, 796.

[53] G. Zheng, H. Mühlenbernd, M. Kenney, G. Li, T. Zentgraf, S. Zhang, *Nat. Nanotechnol.* **2015**, *10*, 308.

[54] P. Chen, L. L. Ma, W. Duan, J. Chen, S. J. Ge, Z. H. Zhu, M. J. Tang, R. Xu, W. Gao, T. Li, W. Hu, Y. Q. Lu, *Adv. Mater.* **2018**, *30*, 1705865.

[55] T. J. White, D. J. Broer, *Nat. Mater.* **2015**, *14*, 1087.

[56] F. Monticone, N. M. Estakhri, A. Alù, *Phys. Rev. Lett.* **2013**, *110*, 203903.

[57] X. Ding, F. Monticone, K. Zhang, L. Zhang, D. Gao, S. N. Burokur, A. de Lustrac, Q. Wu, C. W. Qiu, A. Alù, *Adv. Mater.* **2015**, *27*, 1195.

[58] N. Bozinovic, Y. Yue, Y. Ren, M. Tur, P. Kristensen, H. Huang, A. E. Willner, S. Ramachandran, *Science* **2013**, *340*, 1545.

[59] L. W. Luo, N. Ophir, C. P. Chen, L. H. Gabrielli, C. B. Poitras, K. Bergmen, M. Lipson, *Nat. Commun.* **2014**, *5*, 3069.

[60] W. Ji, C. H. Lee, P. Chen, W. Hu, Y. Ming, L. Zhang, T. H. Lin, V. Chigrinov, Y. Q. Lu, *Sci. Rep.* **2016**, *6*, 25528.

[61] J. Kobashi, H. Yoshida, M. Ozaki, *Nat. Photonics* **2016**, *10*, 389.

[62] H. S. Ee, R. Agarwal, *Nano Lett.* **2016**, *16*, 2818.

[63] P. Gutruf, C. Zou, W. Withayachumnankul, M. Bhaskaran, S. Sriram, C. Fumeaux, *ACS Nano* **2016**, *10*, 133.

1902124 (8 of 8)